Spencer Christopher (Orcid ID: 0000-0003-4264-3701)
Hoiland Carl, William (Orcid ID: 0000-0002-3360-3460)
Evans Noreen (Orcid ID: 0000-0002-7615-8328)

Rapid exhumation of Earth's youngest exposed granites driven by subduction of an oceanic arc

C.J. Spencer[1], M. Danišík[2], H. Ito[3], C. Hoiland[4], S. Tapster[5], H. Jeon[6*], B. McDonald[2], N.J. Evans[1,2]

[1] Earth Dynamics Research Group, The Institute of Geoscience Research, School of Earth and Planetary Sciences, Curtin University, Perth, WA, Australia

[2] John de Laeter Centre, The Institute of Geoscience Research, Curtin University, Perth, WA, Australia

[3] Geosphere Science Sector, Central Research Institute of Electric Power Industry, Chiba, 270-1194, Japan

[4] Department of Geological Sciences, Stanford University, Stanford, CA, USA

[5] NERC Isotope Geosciences Facilities, British Geological Survey, Keyworth, Nottingham NG12 5GG, UK

[6] Centre for Microscopy, Characterisation and Analysis, University of Western Australia, Perth, WA, Australia

Corresponding author: C.J. Spencer (cspencer@curtin.edu.au)

* now at the Swedish Museum of Natural History, Box 50 007, SE-104 05 Stockholm, Sweden

Key Points:

- Timing of crystallization and exhumation of the youngest exposed plutons are constrained with high precision analytical techniques.
- One of the highest exhumation rates for plutonic rocks worldwide are reported.
- Exhumation of Pleistocene granitoid plutons driven by subducting Izu-Bonin oceanic arc.
- Subduction of oceanic arcs drives lithospheric exhumation creates regional-scale thermochronological "hot spots".

This is the author manuscript accepted for publication and has undergone full peer review but has not been through the copyediting, typesetting, pagination and proofreading process, which may lead to differences between this version and the Version of Record. Please cite this article as doi: 10.1029/2018GL080579

Abstract

Exhumation of plutonic systems is driven by a range of mechanisms including isostatic, tectonic, and erosional processes. Variable rates of plutonic exhumation in active subduction systems may be driven by idiosyncrasies of regional geology or by first-order tectonic features. We report new age, isotope, and low-temperature thermochronology constraints of granitoids from the Hida Mountains of central Japan that constrain the highest rates and magnitude of plutonic rock exhumation within the Japan and one of the highest worldwide. This extreme exhumation is centered on the apex of a lithospheric scale anticlinorium associated with the subduction of the Izu-Bonin oceanic arc. The spatial and temporal relationship between the exhumation of these Pleistocene plutons and the subducting/accreting Izu-Bonin oceanic arc links the plate-scale geodynamics and regional exhumation patterns. Identifying thermochronological anomalies within magmatic arcs provides an opportunity to identify ancient asperities previously subducted and responsible for rapid exhumation rates within ancient subduction systems.

Plain Language Summary

Plutonic rocks reach the surface through a variety of geological processes. Generally, this is driven by active tectonic and erosive forces. We provide high-precision geochronological constraint on the youngest exposed subduction zone plutons found in the Hida Mountains of Japan that are 818.5 ± 9.6 thousand years old. Regionally, the Hida Mountains is identified as a thermochronological "hot spot" where the rocks in the region came to the surface very rapidly within the past ~300 thousand years. The exhumation of these plutons was driven by the subduction of the Izu-Bonin oceanic arc.

1 Introduction

Rates of exhumation of plutonic rocks and processes controlling it vary for different tectonic settings (Herman et al., 2013). In cratonic regions that are characterized by long-term stability and little internal deformation, the exhumation of plutonic rocks is controlled primarily by erosion on the surface and exhumation rates are very low, typically not exceeding few tens of meters per million year (e.g., Danišík et al., 2008; Gleadow et al., 2002). Exhumation of plutonic rocks on plate boundaries, in contrast, is enhanced by tectonic processes whereby exhumation rates often range from several hundreds of meters to a few kilometers per million year (e.g., Danišík et al., 2007; Glotzbach et al., 2010; Thomson et al., 2001). It is often difficult to constrain whether high exhumation rates are achieved primarily through higher erosive potential due to topographic and climatic effects or are instead accomplished through structural mechanisms such as intra-orogenic upper crustal extension and/or mid-crustal isostatic readjustment, for example. Constraints on bedrock exhumation rates are critical in assessing these questions especially in modern settings where comparisons can be made to measurable precipitation rates, mass wasting flux, and surface uplift to better understand the nature of ancient orogenic processes.

The Hida Mountain Range (HMR) is unique in that it contains the youngest exposed plutonic rocks on the planet dated as young as 0.8 Ma (Ito et al., 2017; Ito et al., 2013). This fact together with reported cooling ages of <1 Ma (Yamada, 1999; Yamada and Harayama, 1999) requires extremely rapid exhumation rates, but why this is the case and how exhumation rates vary temporally and spatially in this region remains unresolved (Yamada and Harayama, 1999). The driver of this exhumation is thought to be associated with E-W compression accommodated by the Takasegawa fault that lies parallel to the Itoigawa-Shizuoka Tectonic Line

(ISTL) (Harayama, 2003; Harayama et al., 2003; Ito et al., 2012; Yamada, 1999). Additionally, the Philippine Sea plate is subducting obliquely to the direction of Pacific Plate convergence (Isozaki, 1996). However, the orientation of this major fault zone is parallel to the convergence direction and perpendicular to the major tectonic features associated with the Japanese subduction system (Fig. 1). Thus, the nature of the structural features within and flanking the HMR and their relationship to boundary processes and subducting slab geometry and kinematics within the Japanese subduction zone is unclear.

Thermochronology can constrain the temperature-time histories of rocks so as to model the age and rate of their exhumation to the surface and to better constrain the geometry of structures that may have accommodated some or all of their exhumation. Low-temperature thermochronometers such as zircon and apatite (U-Th)/He systems are optimal for characterizing the upper few kilometers of exhumation paths, whereas high-temperature systems such as zircon U-Pb method helps to pinpoint beginning of the exhumation paths at magmatic temperatures.

In this study, we provide new zircon U-Pb geochronology together with zircon (U-Th)/He (ZHe) and apatite (U-Th)/He (AHe) thermochronological data from igneous bedrocks samples in the HMR that not only provide the most precise geochronology of the region (using ID-TIMS), but also provide constraints on geodynamics of the formation, evolution, and exhumation of the plutonic systems of the HMR. These data provide further implications on spatial exhumation patterns of a complex subduction system that link the regional geology to tectonic-plate scale geodynamic forcings.

2 Geological Setting and Samples

The HMR is one of the highest mountain systems in Japan. It includes several >3000 m peaks and stretches north-south for over 100 km. The HMR lie west of the ISTL (i.e. the Eurasian-North American plate boundary) and is recognized as one of the most active seismotectonic regions of the Japanese islands (Ide, 2001; Mikumo et al., 1988). The HMR are composed predominately of Upper Cretaceous to lower Cenozoic plutonic rocks and Pleistocene to Holocene volcanic rocks with a minor amount of older pre-Cenozoic sedimentary and metamorphic basement. Within the HMR are two major Quaternary plutonic complexes, the Kurobegawa Granite and Takidani Granodiorite. The Kurobegawa granite pluton is exposed over an area of ~100 km^2 and represents the youngest exposed felsic plutonic complex in the world which has previously been dated at ~750 ka (Ito et al., 2017).

The Kurobegawa Granite has a vertical exposure from 700 m to 3000 m and is geochemically and texturally divided into three units (upper, middle, and lower) and is intrusive into the Quaternary Jiigatake felsic volcanic rocks (Harayama et al., 2003; Wada et al., 2004). Our sampling campaign targeted the northern and southern portions of the pluton. Samples, ranging in composition from diorite (enclaves) to granodiorite and granite, were collected from the locality previously identified as hosting the youngest granite plutonic sample on Earth (Ito et al., 2013). The zircon U-Pb ages of granodiorite samples reported by Ito et al. (2017) reproduce and confirm the young age previously reported (Harayama et al., 2010). However, one sample (JP15) was also collected from an aplite dyke that crosscuts the granodiorite previously argued to be the youngest granite.

The Takidani Granodiorite covers ~50 km^2 with vertical exposure from 1450 m to 2670 m in elevation that is elongated along the N-S axis of the HMR. The pluton is compositionally zoned with equigranular biotite-hornblende granodiorite at the base grading towards porphyritic biotite-hornblende granite at the top

(Harayama, 1992; Ito et al., 2017). Two samples were collected from the southern portions of the pluton. Additional samples of Miocene and Paleocene granites were collected within the environs of the Kurobegawa and Takidani plutons (Okukurobe and Oshirasawa). GPS coordinates of sample locations are presented in Table 1.

3 Methods

Collected samples were disaggregated using jaw crusher and disc mill housed at the John de Laeter Centre (JdLC) at Curtin University. Zircon and apatite were extracted using traditional mineral separation techniques (i.e. sieving, Wilfley table, Franz magnetic separation, and lithium polytungstate and diiodomethane heavy liquid separation). Zircon were mounted in epoxy, imaged with cathodoluminescence, and analyzed for δ^{18}O, U-Pb, and Hf via secondary ion mass spectrometry (SIMS; δ^{18}O) at the University of Western Australia and laser ablation inductively coupled plasma mass spectrometry (LA-ICP-MS; U-Pb and Hf) at the JdLC following the methods of Spencer et al. (2017a). Zircon from one sample (JP15) was analyzed with chemical abrasion-isotope dilution-thermal ionization mass spectrometry (CA-ID-TIMS) at the NERC Isotope Geosciences Laboratory (NIGL) of the British Geological Survey following the methods of Condon et al. (2015). Zircon and apatite were analyzed for (U-Th)/He using an Alphachron system and solution ICP-MS at the JdLC and TSW Analytical, respectively, following the methods of Danišík et al. (2012a,b). Full methodology is described in the supplementary material. Summary of data in this study is presented in Table 1.

4 Results

4.1 Zircon U-Pb (LA-ICP-MS)

Ten samples were analyzed via LA-ICP-MS that range in age from ~0.8 to ~64.6 Ma (Fig. 2A). Weighted means and reduced chi-squared values were calculated using KDχ (Spencer, et al., 2017b). Nine samples revealed single populations (as defined by the reduced chi-square test; Spencer et al., 2016) whereas, one sample (JP01) revealed three discrete age populations (~1.4 Ma, ~1.0 Ma, and ~0.8 Ma). Weighted means of the samples fall into five discrete ages, ~0.8 Ma (two samples), ~1.0-1.2 Ma (three samples), ~1.5 Ma (three samples), ~9 Ma (one sample), and ~63 Ma (three samples).

4.2 Zircon U-Pb (CA-ID-TIMS)

Chemically abraded zircon (Mattinson, 2005) from sample JP15 analyzed by ID-TIMS following the method of Tapster et al. (2016) yielded a ^{230}Th corrected ^{206}Pb/^{238}U weighted mean age of 0.8185 ± 0.0087 / 0.0096 Ma (± 2 sigma analytical / total uncertainty; n = 4, MSWD = 0.13) from the youngest population interpreted as best estimate for emplacement. Two additional grains yielded ages of ~0.9 Ma that were excluded from the weighted mean age calculation (Fig. 2A). The ^{230}Th correction adds ~0.09 Ma (from 0.7282 ± 0.0030 to 0.8185 ± 0.0087) to the final age.

4.3 Zircon δ^{18}O and εHf

Zircon δ^{18}O were obtained for eight samples with weighted means of δ^{18}O range from 5.9 ± 0.4‰ to 6.9 ± 0.2‰. When combined with the geochronological data, the δ^{18}O values increase from the Paleocene- to

Quaternary-age samples (Fig. 2B). Zircon εHf was obtained for the same samples as $\delta^{18}O$ whose weighted means range from -0.4 ± 0.3 to -4.6 ± 0.3 and decrease through time (Fig. 2B).

4.4 Zircon and Apatite (U-Th)/He

Single zircon grains (n=60) from nine and apatite single grains (n=19) from four samples were dated by (U-Th)/He method. Average zircon and apatite (U-Th)/He ages corrected for alpha ejection (Farley et al., 1996) range from ~7.8 Ma to ~370 kyr and from ~650 kyr to ~289 kyr, respectively (Fig. 1). See Supplementary Figure 1 for modelled time-temperature diagrams showing thermal trajectories reproducing measured (U-Th)/He ages of the samples.

5 Discussion

Geochronologic data has previously been reported from the Kurobegawa and Takidani plutons highlighting the fact these plutons are the youngest currently known on the planet (Harayama, 1992; Harayama, 1994; Ito et al., 2017; Ito et al., 2013; Yamada and Harayama, 1999). Previously published thermochronologic data of the Takidani pluton based on whole rock and biotite Rb-Sr, biotite and hornblende K-Ar, and zircon fission track dating methods also identified the HMR as representing a region of rapid exhumation (Harayama, 1992; Harayama, 1994; Yamada and Harayama, 1999). The high-precision CA-ID-TIMS zircon U-Pb analyses of the youngest phase of magmatism of the Kurobegawa plutonic system support this with a final age of 818.5 ± 9.6 kyr (Fig. 2). The Quaternary magmatism in the HMR appears to have occurred in three discrete pulses at ~2.3 Ma, ~1.6 Ma and 0.9 Ma evidenced by analysis of detrital zircon in modern rivers (Ito et al., 2017). The LA-ICP-MS zircon U-Pb analyses also confirm the used ages of Quaternary pulses of magmatism as well as previous episodes of magmatism extending back to the early Paleogene (Fig. 2).

The zircon $\delta^{18}O$ and εHf data presented herein provides insight into the genesis and evolution of the plutonic systems of the HMR. The oldest magmatism in the HMR displays moderately elevated $\delta^{18}O$ and unradiogenic εHf implying an elevated degree of reworking older crust (average depleted mantle model age = ~1200 Ma). The εHf signatures subsequently decrease through time and $\delta^{18}O$ increase through time, with the Paleocene phase of magmatism representing the most mantle-like $\delta^{18}O$ and most radiogenic εHf implying an increased amount of crustal recycling with time. This potentially signals the increased reworking of subducted supracrustal material from the Izu-Bonin Arc.

The new ZHe and AHe data constrain the timing of cooling of the samples through the ~225°C and ~95°C isotherms (assuming 60 μm radius equivalent sphere and the measured average cooling rate of 500 °C/km; Farley, 2002; Reiners et al., 2004), respectively, related to the exhumation of the plutons in the HMR. ZHe data suggest that central part of the range (sample JP12) reached the depths of ~3.0 km at 1.1 Ma (here and elsewhere the values were calculated by assuming a geothermal gradient of ~70°C/km (average values from the HMR as reported by Tanaka et al. (2004) and surface temperature of 10°C)), whereas the northern and southern parts of the pluton at 790-370 kyr. AHe data suggest that central part of the pluton reached the depths of ~1.2 km at 650-580 kyr and southern part arrived at ~1.2 km depths at 290 kyr. These AHe ages document final exhumation of HMR plutons in the Middle Pleistocene and, together with two ages from Namche Barwa Syntaxis (Yang et al., 2018), represent the youngest cooling ages ever reported for basement rocks worldwide.

The contrasting tectonic settings responsible for these exceptionally young cooling ages (oceanic subduction and continental collision) implies the rapid exhumation rates are not confined to continent collisional settings.

High-temperature U-Pb and low-temperature (U-Th)/He data allow reconstruction of complete cooling trajectories for the samples from their crystallization to their exhumation to the surface (Fig. 3), and the obtained cooling trajectories in combination with assumed geothermal gradients can be in turn used to calculate not only the rates but also the magnitude of exhumation. Our data for <1.6 Ma granites suggests that some portions of HMR plutons were exhumed from depths of <24 km to subsurface levels in 400 kyr at rates ranging from 20 up to 40 mm/yr (km/Ma; assuming a minimum of 25 °C/km; 5 to 10 mm/yr (km/Ma) if 100 °C/km is assumed; 25 °C/km and 100 °C/km are minimum and maximum values of geothermal gradient of the HMR reported by Tanaka et al., 2004). These extremely high exhumation rates and magnitudes are one of the greatest values thus far documented for granites by geochronological data. It is likely, however, that a portion of the extreme cooling paths documented between zircon U-Pb ages of crystallization and ZHe age reflects rapid initial cooling due to emplacement of the magma at relatively shallow depths and thus will need to be amended as future studies provide better constraints on emplacement depth.

Our new constraints can be compared to previous estimates of exhumation in the HMR and regionally. Terrestrial *in situ* cosmogenic nuclides were previously used to estimate denudation rates in the HMR ranging from 0.2 to 7.0 mm/yr (Matsushi et al., 2014), which are significantly lower than the exhumation rates presented in this study. This slight difference can be explained by the fact that cosmogenic nuclides record denudation moderated by surface processes rather than tectonic processes that are recorded by high- and low-temperature thermochronometeres presented here (Vance et al., 2003). Maximum uplift in the HMR during the Quaternary was estimated to be approximately 1700 m by measuring the elevation of low-relief erosional surfaces assumed to represent uplifted remnants of peneplains established by late Neogene time at near sea-level (Research Group for Quaternary Tectonic Map, 1968). It is possible that the maximum uplift of ~1700 m is underestimated because this study did not account for denudation and neglected the possibility of high-altitude denudation surfaces were potentially formed by periglacial processes (Sugai, 1990, 1995). Low-temperature thermochronology data have also been used in southern part of the Northeast Japan Arc (Fig. 4), to estimate exhumation rates as being <0.1 mm/yr in the forearc region, ~0.1 to 1 mm/yr along the volcanic front, and ~0.1 to 0.3 mm/yr in the backarc region (Sueoka et al., 2017).

The HMR lies parallel to the ISTL which is likely the primary fault system controlling the exhumation of the Quaternary plutonic rocks (Harayama, 1992; Ito et al., 2013; Wada, 2004). ISTL is a complex active thrust fault system that thrusts the crustal block of the HMR to the east (Sagiya et al., 2002, 2004). Slip rates along the thrust fault systems associated with the Itoigawa-Shizuoka Tectonic Line is estimated as high as ~9 mm/yr (Ikeda & Yonekura, 1986).

Importantly, the ISTL lies along the apex of a large anticlinorium within the Izu collision zone (Fig. 4). The collision of the Izu-Bonin arc with the Honshu arc has resulted in the deformation of the major tectonic boundaries in central Honshu and the subduction of the Izu-Bonin arc and the buoyant nature of the subducting oceanic arc is likely the direct cause of the exhumation in the HMR (Yamamoto et al., 2009).

The spatially diverse exhumation of the Honshu arc (Fig. 4) may provide a useful framework in constraining the subduction of crust thicker than normal oceanic crust (e.g. oceanic arcs, ocean islands, mid-ocean ridges). We would predict that regions where thicker than normal oceanic crust has subduction would have experienced higher than normal exhumation. For example, the subduction of the Nazca Ridge beneath the Andes of South America has resulted in ~5 km exhumation of the Fitzcarrald Arch (Bishop et al., 2018; Espurt et al., 2010). Although the basement rocks are not yet exposed at the surface in the Fitzcarrald Arch, our model would predict the basement rocks beneath the sedimentary cover would exhibit younger exhumation ages than the basement north and south of the where the Nazca Ridge is subducting.

Exhumation anomalies in subduction zones around the world merit further consideration for their potential as geothermal resources. Additionally, campaign-style thermochronological investigations of ancient subduction zones may provide insight into the reconstruction of the oceanic crust and whether exhumation 'hot spots' as seen in the HMR indicate the subduction of thicker-than-normal oceanic crust.

Acknowledgments

The authors thank two anonymous reviewers for providing helpful and constructive comments. GeoHistory Facility instruments (part of the John de Laeter Centre) were funded via an Australian Geophysical Observing System (AGOS) grant provided to AuScope by the AQ44 Australian Education Investment Fund. The Australian Microscopy and Microanalysis Research Facility, AuScope, the Australian Science and Industry Endowment Fund, and the State Government of Western Australia contributed funding to Centre for Microscopy, Characterisation and Analysis at the University of Western Australia. M.D. was supported by Australian Research Council (ARC) Discovery funding scheme (DP160102427), and C.S. and M.D. were supported by Curtin Research Fellowship. M.D. thanks C. May for help with solution ICP-MS analyses, I. Dunkl for sharing PepiFLEX software for ICP-MS data reduction and A. Frew for help with mineral dissolution.

The authors affirm there is no real or perceived financial conflicts of interests.

The full dataset supporting the conclusions can be obtained in the online supplementary materials.

References

Bishop, B. T., Beck, S. L., Zandt, G., Wagner, L. S., Long, M. D., & Tavera, H. (2018). Foreland uplift during flat subduction: Insights from the Peruvian Andes and Fitzcarrald Arch. Tectonophysics, 731, 73–84.

Condon, D. J., Schoene, B., McLean, N. M., Bowring, S. A., & Parrish, R. R. (2015). Metrology and traceability of U-Pb isotope dilution geochronology (EARTHTIME Tracer Calibration Part I). Geochimica et Cosmochimica Acta, 164, 464–480.

Danišík, M., Kuhlemann, J., Dunkl, I., Székely, B., & Frisch, W. (2007). Burial and exhumation of Corsica (France) in the light of fission track data. Tectonics, 26(1).

Danišík, M., Sachsenhofer, R. F., Privalov, V. A., Panova, E. A., Frisch, W., & Spiegel, C. (2008). Low-temperature thermal evolution of the Azov Massif (Ukrainian Shield – Ukraine) – Implications for interpreting (U–Th)/He and fission track ages from cratons. Tectonophysics, 456(3–4), 171–179.

Danišík, M., Štěpančíková, P., & Evans, N. J. (2012a). Constraining long-term denudation and faulting history in intraplate regions by multisystem thermochronology: An example of the Sudetic Marginal Fault (Bohemian Massif, central Europe). Tectonics, 31(2).

Danišík, M., Kuhlemann, J., Dunkl, I., Evans, N.J., Székely, B. and Frisch, W. (2012b). Survival of ancient landforms in a collisional setting as revealed by combined fission track and (U-Th)/He thermochronometry: A case study from Corsica (France). The Journal of Geology, 120(2), 155–173.

Espurt, N., Baby, P., Brusset, S., Roddaz, M., Hermoza, W., & Barbarand, J. (2010). The Nazca Ridge and uplift of the Fitzcarrald Arch: implications for regional geology in northern South America. Amazonia, Landscape and Species Evolution: A Look into the Past. Blackwell-Wiley, 89–100.

Farley, K. A. (2002). (U-Th)/He dating: Techniques, calibrations, and applications. Reviews in Mineralogy and Geochemistry, 47(1), 819–844.

Farley, K. A., Wolf, R. A., & Silver, L. T. (1996). The effects of long alpha-stopping distances on (U-Th)/He ages. Geochimica et Cosmochimica Acta, 60(21), 4223–4229.

Gleadow, A. J. W., Kohn, B. P., Brown, R. W., O’Sullivan, P. B., & Raza, A. (2002). Fission track thermotectonic imaging of the Australian continent. Tectonophysics, 349(1–4), 5–21.

Glotzbach, C., Reinecker, J., Danišík, M., Rahn, M., Frisch, W., & Spiegel, C. (2010). Thermal history of the central Gotthard and Aar massifs, European Alps: Evidence for steady state, long-term exhumation. Journal of Geophysical Research: Earth Surface, 115(F3).

Harayama, S. (1992). Youngest exposed granitoid pluton on Earth: cooling and rapid uplift of the Pliocene-Quaternary Takidani Granodiorite in the Japan Alps, central Japan. Geology, 20(7), 657–660. https://doi.org/10.1130/0091-7613(1992)020<0657:YEGPOE>2.3.CO;2

Harayama, S. (1994). Cooling history of the youngest exposed pluton in the World: The Plio-Pleistocene Takidani granodiorite (Japan Alps, central Japan). Memoirs of the Geological Society of Japan, 43, 87–97.

Harayama, S. (2003). Quaternary and Pliocene granites in the Northern Japan Alps. In Hutton Symposium V, Field Guidebook.

Harayama, S., Ohyabu, K., Miyama, Y., Adachi, H., & Shukuwa, R. (2003). Eastward tilting and uplifting after the late Early Pleistocene in the eastern-half area of the Hida Mountain Range. The Quaternary Research (Daiyonki-Kenkyu), 42(3), 127–140.

Harayama, S., Takahashi, M., Shukuwa, R., Itaya, T., & Yagi, K. (2010). High-temperature hot springs and Quaternary Kurobegawa Granite along the Kurobegawa River. J. Geol. Soc. Japan, 116, 63–81.

Hasebe, N., Suwargadi, B.W., & Nishimura, S. (2000). Fission track ages of the Omine acidic rocks, Kii Peninsula, Southwest Japan. Geochemical Journal, 34(3), 229–235.

Herman, F., Seward, D., Valla, P. G., Carter, A., Kohn, B., Willett, S. D., & Ehlers, T. A. (2013). Worldwide acceleration of mountain erosion under a cooling climate. Nature, 504(7480), 423.

Holtz, F., & Johannes, W. (1994). Maximum and minimum water contents of granitic melts: implications for chemical and physical properties of ascending magmas. Lithos, 32(1–2), 149–159.

Ide, S. (2001). Complex source processes and the interaction of moderate earthquakes during the earthquake swarm in the Hida-Mountains, Japan, 1998. Tectonophysics, 334(1), 35–54.

Ikeda, Y., & Yonekura, N. (1986). Determination of late Quaternary rates of net slip on two major fault zones in central Japan. Bull. Dept. Geogr. Univ. Tokyo, 18, 49–63.

Isozaki, Y. (1996). Anatomy and genesis of a subduction-related orogen: A new view of geotectonic subdivision and evolution of the Japanese Islands. Island Arc, 5(3), 289–320.

Ito, H., & Tanaka, K. (1999). Radiometric age determination on some granitic rocks in the Hida Range, central Japan. Remarkable age difference across a fault. Geological Journal, 105(4), 241–246.

Ito, H., Tamura, A., Morishita, T., & Arai, S. (2012). Timing of some plutonic intrusions and tectonics in the Hida Mountain Range: An application of LA-ICP-MS U-Pb dating on zircons. J. Geol. Soc. Japan, 118, 449–456.

Ito, H., Yamada, R., Tamura, A., Arai, S., Horie, K., & Hokada, T. (2013). Earth's youngest exposed granite and its tectonic implications: The 10-0.8 Ma Kurobegawa Granite. Scientific Reports, 3, 1–5.

Ito, H., Spencer, C. J., Danišík, M., & Hoiland, C. W. (2017). Magmatic tempo of Earth's youngest exposed plutons as revealed by detrital zircon U-Pb geochronology. Scientific Reports, 7(1).

Kamp, P.J., & Takemura, K. (1993). Thermo-tectonic history of Ryoke Basement in Hohi volcanic zone, northeast Kyushu, Japan: Constraints from fission track thermochronology. Island Arc, 2(4), 213–227.

Kiminami, K., & Imaoka, T. (2013). Spatiotemporal variations of Jurassic–Cretaceous magmatism in eastern Asia (Tan-Lu Fault to SW Japan): evidence for flat-slab subduction and slab rollback. Terra Nova, 25(5), 414–422.

Luth, W. C., Jahns, R. H., & Tuttle, O. F. (1964). The granite system at pressures of 4 to 10 kilobars. Journal of Geophysical Research, 69(4), 759–773.

Matsushi et al. (2014) Jour. Japan Soc. Eng. Geol., 54, 272-280 (in Japanese with English abstract).

Mattinson, J. M. (2005). Zircon U-Pb chemical abrasion ("CA-TIMS") method: Combined annealing and multi-step partial dissolution analysis for improved precision and accuracy of zircon ages. Chemical Geology, 220(1–2), 47–66.

Mikumo, T., Wada, H., & Makoto, K. (1988). Seismotectonics of the Hida region, central Honshu, Japan. Tectonophysics, 147(1–2), 95–119.

Page, F. Z., Fu, B., Kita, N. T., Fournelle, J., Spicuzza, M. J., Schulze, D. J., et al. (2007). Zircons from kimberlite: New insights from oxygen isotopes, trace elements, and Ti in zircon thermometry. Geochimica et Cosmochimica Acta, 71(15), 3887–3903.

Reiners, P. W., Spell, T. L., Nicolescu, S., & Zanetti, K. A. (2004). Zircon (U-Th)/He thermochronometry: He diffusion and comparisons with 40Ar/39Ar dating. Geochimica et Cosmochimica Acta, 68(8), 1857–1887.

Research Group for Quaternary Tectonic Map (1968). Quaternary Research (Daiyonki Kenkyu). 7, 182-187 (in Japanese with English abstract).

Sagiya, T., Nishimura, T., Iio, Y., & Tada, T. (2002). Crustal deformation around the northern and central Itoigawa-Shizuoka Tectonic Line. Earth, Planets and Space, 54(11), 1059–1063.

Sagiya, T., Nishimura, T., & Iio, Y. (2004). Heterogeneous crustal deformation along the central-northern Itoigawa-Shizuoka tectonic line fault system, central Japan. Earth, Planets and Space, 56(12), 1247–1252.

Spencer, C. J., Kirkland, C. L., & Taylor, R. J. M. (2016). Strategies towards statistically robust interpretations of in situ U-Pb zircon geochronology. Geoscience Frontiers, 7(4), 581–589. https://doi.org/10.1016/j.gsf.2015.11.006

Spencer, C. J., Cavosie, A. J., Raub, T. D., Rollinson, H., Jeon, H., Searle, M. P., et al. (2017a). Evidence for melting mud in Earth's mantle from extreme oxygen isotope signatures in zircon. Geology, 45(11). https://doi.org/10.1130/G39402.1

Spencer, C. J., Yakymchuk, C., & Ghaznavi, M. (2017b). Visualising data distributions with kernel density estimation and reduced chi-squared statistic. Geoscience Frontiers, 8(6). https://doi.org/10.1016/j.gsf.2017.05.002

Sueoka, S., Kohn, B. P., Tagami, T., Tsutsumi, H., Hasebe, N., Tamura, A., & Arai, S. (2012). Denudation history of the Kiso Range, central Japan, and its tectonic implications: Constraints from low-temperature thermochronology. Island Arc, 21(1), 32–52. https://doi.org/10.1111/j.1440-1738.2011.00789.x

Sueoka, S., Tagami, T., & Kohn, B. P. (2017). First report of (U-Th)/He thermochronometric data across Northeast Japan Arc: Implications for the long-term inelastic deformation Crustal Dynamics: Unified Understanding of Geodynamics Processes at Different Time and Length Scales Yoshihisa Iio, Richard. Earth, Planets and Space, 69(1).

Sugai, T. (1990). The origin and geomorphic characteristics of the erosional low-relief surfaces in the Akaishi Mountains and the southern part of the Mikawa plateau, central Japan. Geographical Review of Japan A, 63, 793–813.

Sugai, T. (1995). Origin of the low-relief surfaces on ridges in the Kiso range and northern part of the Mino-Mikawa plateau, central Japan. Proceedings of the Department of Humanities, College of General Education, University of Tokyo. Series of Human Geography, 7, 1–40.

Tagami, T. and Shibata, K. (1993). Fission track ages on some Ryoke granitic rocks along the Median Tectonic Line, Southwest Japan. Geochemical Journal, 27(6), 403–406.

Tanaka, A., Yamano, M., Yano, Y., & Sasada, M. (2004). Geothermal gradient and heat flow data in and around Japan (I): Appraisal of heat flow from geothermal gradient data. Earth, Planets and Space, 56(12), 1191–1194.

Tapster, S., Condon, D. J., Naden, J., Noble, S. R., Petterson, M. G., Roberts, N. M. W., et al. (2016). Rapid thermal rejuvenation of high-crystallinity magma linked to porphyry copper deposit formation; evidence from the Koloula Porphyry Prospect, Solomon Islands. Earth and Planetary Science Letters, 442, 206–217.

Thomson, S. N., Hervé, F., & Stöckhert, B. (2001). Mesozoic-Cenozoic denudation history of the Patagonian Andes (southern Chile) and its correlation to different subduction processes. Tectonics, 20(5), 693–711.

Vance D., Bickle M., Ivy-Ochs S. and Kubik P. W. (2003) Erosion and exhumation in the Himalaya from cosmogenic isotope inventories of river sediments. Earth Planet. Sci. Lett. 206, 273–288.

Wada, H. (2004). Mafic enclaves densely concentrated in the upper part of a vertically zoned felsic magma chamber: The Kurobegawa granitic pluton, Hida Mountain Range, central Japan, (7), 788–801.

Wada, H., Harayama, S., & Yamaguchi, Y. (2004). Mafic enclaves densely concentrated in the upper part of a vertically zoned felsic magma chamber: The Kurobegawa granitic pluton, Hida Mountain Range, central Japan. Bulletin of the Geological Society of America, 116(7–8), 788–801.

Yamada, R. (1999). Cooling history analysis of granitic rock in the Northern Alps, central Japan. The Earth Monthly, 21, 803–810.

Yamada, R. and Harayama, S. (1999). Fission track and K-Ar dating on some granitic rocks of the Hida Mountain Range, central Japan. Geochemical journal, 33(1), 59–66.

Yamada, K., & Tagami, T. (2008). Postcollisional exhumation history of the Tanzawa Tonalite Complex, inferred from (U-Th)/He thermochronology and fission track analysis. Journal of Geophysical Research: Solid Earth, 113(B3).

Yamaji, A. (2003). Slab rollback suggested by latest Miocene to Pliocene forearc stress and migration of volcanic front in southern Kyushu, northern Ryukyu Arc. Tectonophysics, 364(1–2), 9–24.

Yamamoto, S., Senshu, H., Rino, S., Omori, S., & Maruyama, S. (2009). Granite subduction □: Arc tectonic erosion and sediment subduction, 15, 443–453. https://doi.org/10.1016/j.gr.2008.12.009

Yang, R., Herman, F., Fellin, M. G., & Maden, C. (2018). Exhumation and topographic evolution of the Namche Barwa Syntaxis, eastern Himalaya. Tectonophysics, 722, 43–52.

Yuguchi, T., Amano, K., Tsuruta, T., Danhara, T., & Nishiyama, T. (2011). Thermochronology and the three-dimensional cooling pattern of a granitic pluton: an example from the Toki granite, Central Japan. Contributions to Mineralogy and Petrology, 162(5), 1063–1077.

Yuguchi, T., Sueoka, S., Iwano, H., Danhara, T., Ishibashi, M., Sasao, E., & Nishiyama, T. (2017). Spatial distribution of the apatite fission-track ages in the Toki granite, central Japan: Exhumation rate of a Cretaceous pluton emplaced in the East Asian continental margin. Island Arc, 26(6), e12219.

Figure 1. A) Simplified map of the Hida Mountain Range (HMR) (after Ito et al., 2017). ISTL: Itoigawa-Shizuoka Tectonic Line, MTL: Median Tectonic Line. B) Topographic map of the sampling region of the HMR with sample locations and geo- and thermochronological data from this study. All uncertainties are given at 2 sigma and include systematic uncertainty (2%). C) Simplified geologic map of the HMR (after Ito et al., 2013).

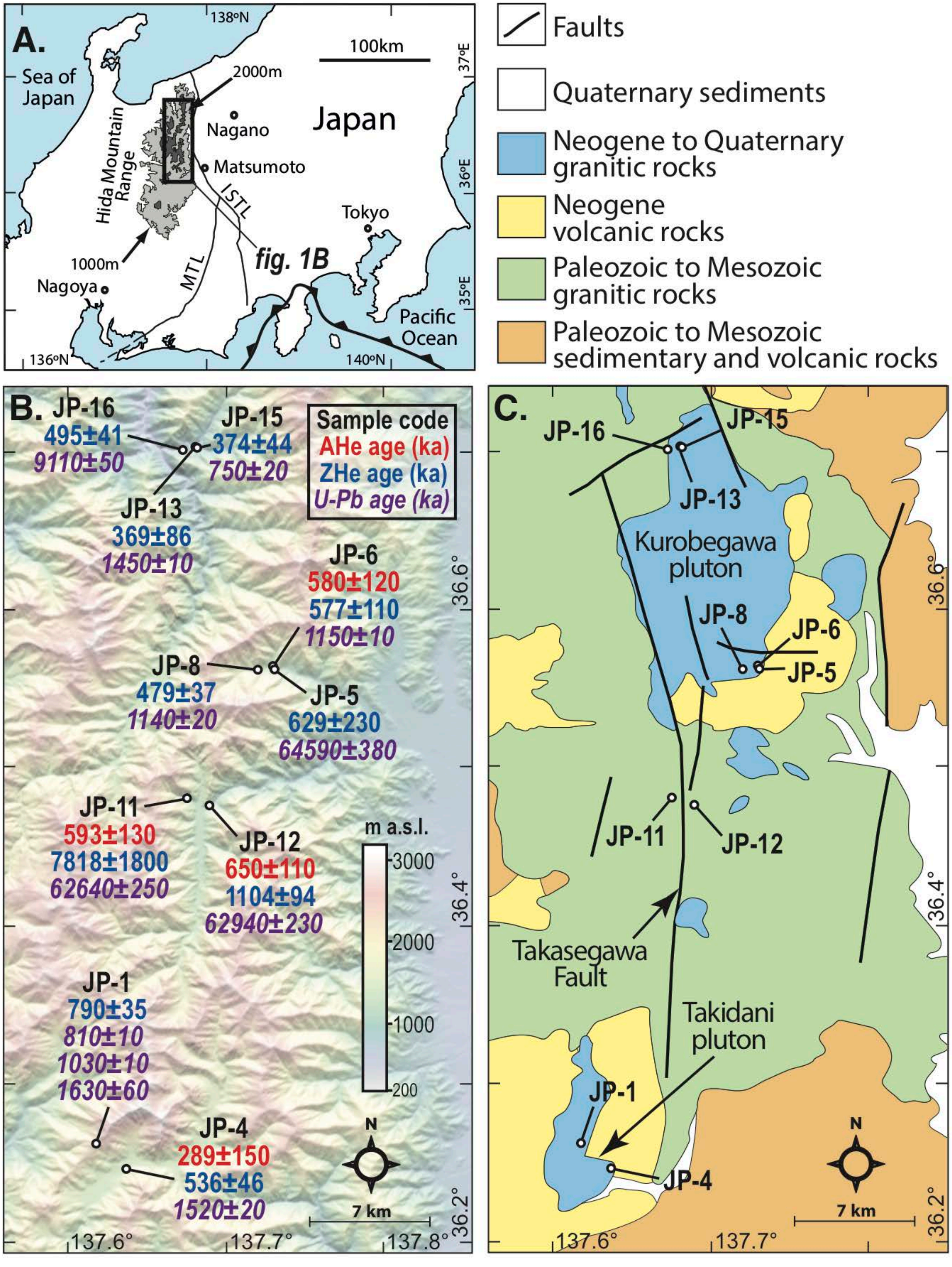
Faults
Quaternary sediments
Neogene to Quaternary granitic rocks
Neogene volcanic rocks
Paleozoic to Mesozoic granitic rocks
Paleozoic to Mesozoic sedimentary and volcanic rocks
A.
138ºN
100km
37ºE
Sea of Japan
2000m
Japan
Nagano
Hida Mountain Range
Matsumoto
36ºE
ISTL
Tokyo
1000m
fig. 1B
MTL
Nagoya
35ºE
Pacific Ocean
136ºN
140ºN
B.
JP-16
495±41
9110±50
JP-15
374±44
750±20
Sample code
AHe age (ka)
ZHe age (ka)
U-Pb age (ka)
JP-13
369±86
1450±10
JP-6
580±120
577±110
1150±10
36.6°
JP-8
479±37
1140±20
JP-5
629±230
64590±380
JP-11
593±130
7818±1800
62640±250
JP-12
650±110
1104±94
62940±230
m a.s.l.
3000
2000
1000
200
36.4°
JP-1
790±35
810±10
1030±10
1630±60
JP-4
289±150
536±46
1520±20
N
7 km
36.2°
137.6°
137.7°
137.8°
C.
JP-16
JP-15
JP-13
Kurobegawa pluton
36.6°
JP-8
JP-6
JP-5
JP-11
JP-12
36.4°
Takasegawa Fault
Takidani pluton
JP-1
JP-4
N
7 km
36.2°
137.6°
137.7°

Figure 2. A) Zircon U-Pb data from the HMR granitoid samples of Paleocene, Miocene, and Pleistocene age, respectively. All samples were analyzed with LA-ICP-MS and JP15 was also analyzed by ID-TIMS. Sample JP01 had multiple age populations. B) Zircon O- and Hf- isotope compositions (shown at 2-sigma) plotted against U-Pb age (note the log-scale). Mantle $\delta^{18}O$ compositional range is from Page et al. (2007). εHf values are shown as initial ratios at time of crystallization ($\varepsilon Hf_{initial}$). CHUR: Chondrite Uniform Reservoir.

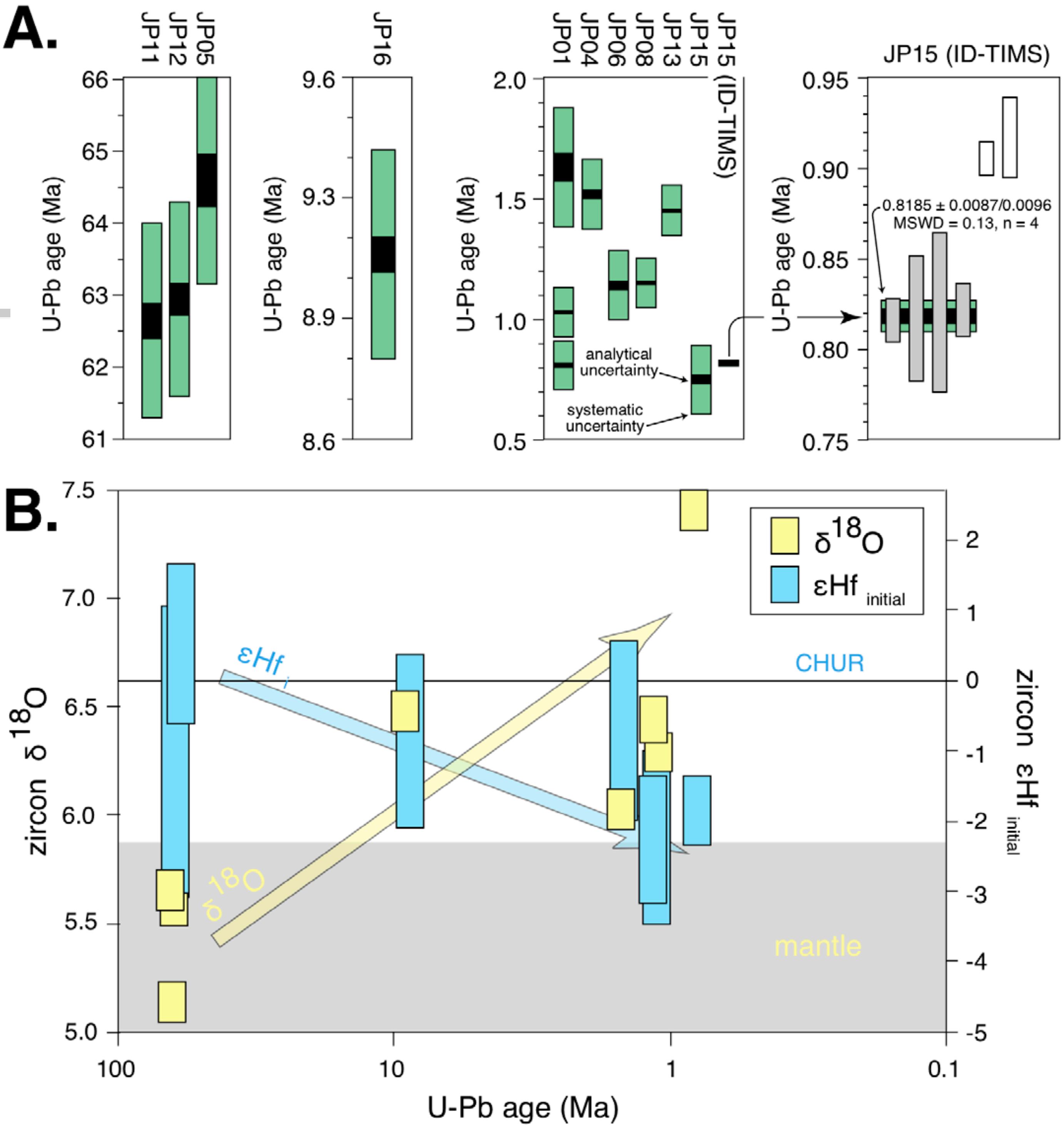
A.
JP11
JP12
JP05
JP16
JP01
JP04
JP06
JP08
JP13
JP15
JP15 (ID-TIMS)
JP15 (ID-TIMS)
U-Pb age (Ma)
66
65
64
63
62
61
9.6
9.3
8.9
8.6
2.0
1.5
1.0
0.5
0.95
0.90
0.85
0.80
0.75
analytical uncertainty
systematic uncertainty
0.8185 ± 0.0087/0.0096
MSWD = 0.13, n = 4
B.
zircon δ18O
7.5
7.0
6.5
6.0
5.5
5.0
zircon εHf initial
2
1
0
-1
-2
-3
-4
-5
δ18O
εHf initial
εHf i
CHUR
δ18O
mantle
100
10
1
0.1
U-Pb age (Ma)

Figure 3. Time-temperature exhumation paths for the HMR granitoids as constrained by zircon and apatite geo-/thermochronological data and assuming a geothermal gradient of 25°C/km and 100°C/km (Tanaka et al., 2004) and zircon crystallization of 600°C, i.e. the approximate minimum temperature of the granite wet solidus (Holtz & Johannes, 1994; Luth et al., 1964). If the true zircon crystallization temperature were higher, the exhumation rates would be higher and if the geothermal gradient were higher, the exhumation rates would be lower.

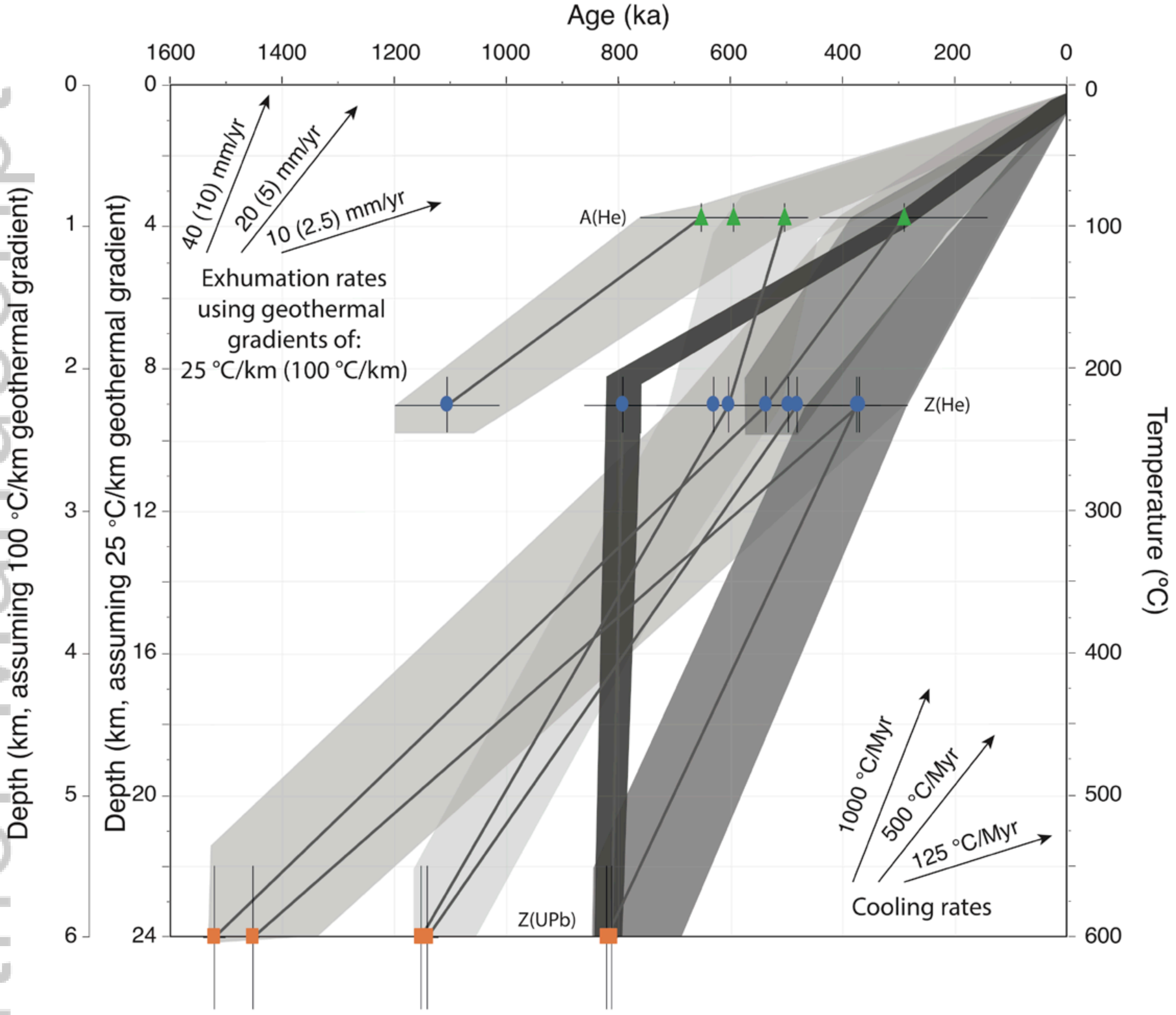

Figure 4. A) Spatial interpolation (inverse distance weighting) of compiled zircon and apatite fission track (ZFT and AFT, respectively) and ZHe and AHe data from Japan. Volcanic and sedimentary samples are excluded from this compilation. There is a clear zone of high exhumation that is centered on the HMR. Data are compiled from Yamada and Harayama, 1999; Ito and Tanaka, 1999; Tagami and Shibata, 1993; Hasebe et al. 2000; Kamp and Takemura, 1993; Yuguchi et al. 2011, 2017; Yamada and Tagami, 2008; Sueoka et al., 2012, 2017; and this study. B) Simplified map of the major tectonic structures of central Japan (Yamamoto et al., 2009). Importantly, these structures are either caused or heavily modified by the collision and accretion/subduction of the Izu-Bonin oceanic arc. The HMR lies directly in line with the trajectory of the Izu-Bonin oceanic arc that is likely the direct cause of the fast exhumation of the HMR. In all cases, the apatite He ages are younger than the zircon He ages. The apparent contradiction to this relationship seen in the regions without data is due to interpolation methods.

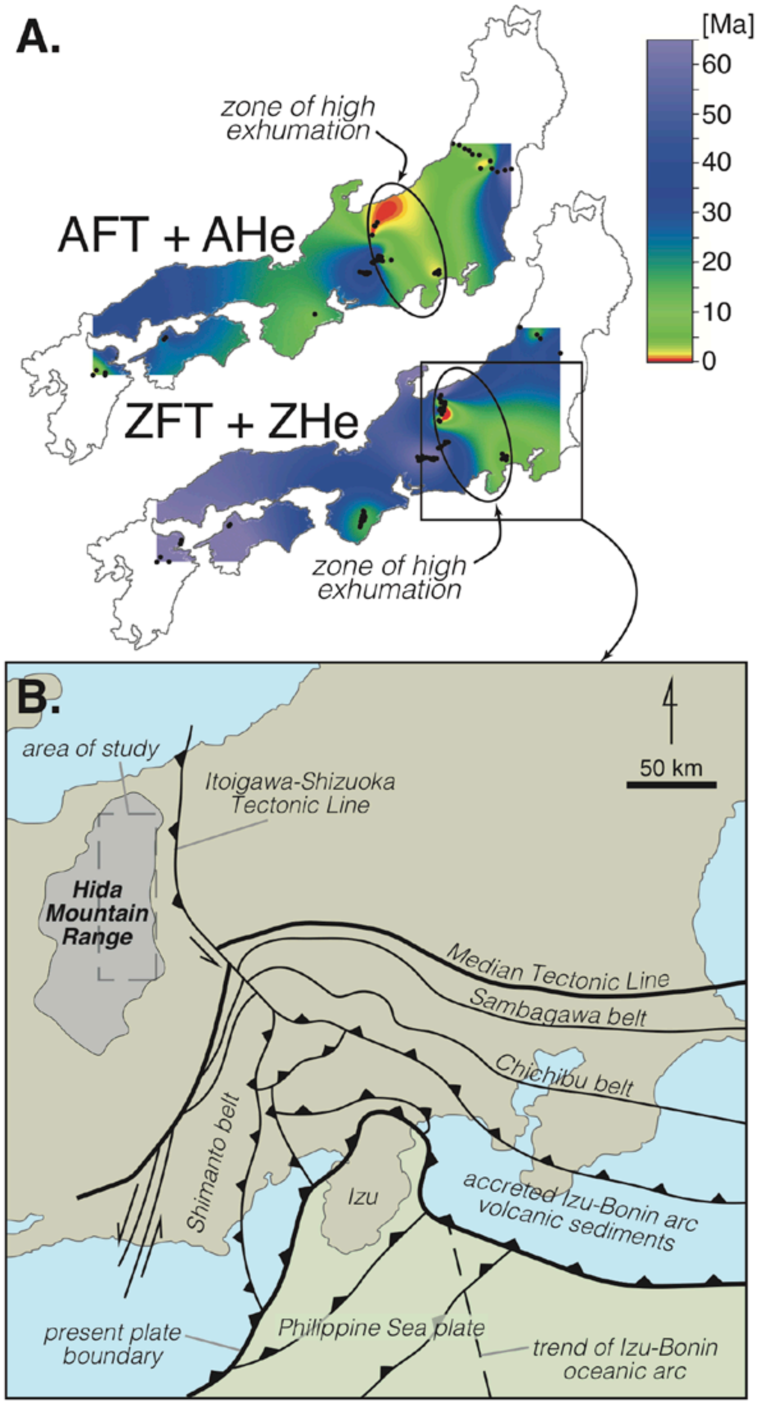
A.
zone of high exhumation
AFT + AHe
ZFT + ZHe
zone of high exhumation
[Ma]
60
50
40
30
20
10
0
B.
area of study
Itoigawa-Shizuoka Tectonic Line
Hida Mountain Range
50 km
Median Tectonic Line
Sambagawa belt
Chichibu belt
Shimanto belt
Izu
accreted Izu-Bonin arc volcanic sediments
present plate boundary
Philippine Sea plate
trend of Izu-Bonin oceanic arc

Table 1. Sample information, GPS localities, geo- and thermochronological summary, and isotopic data.

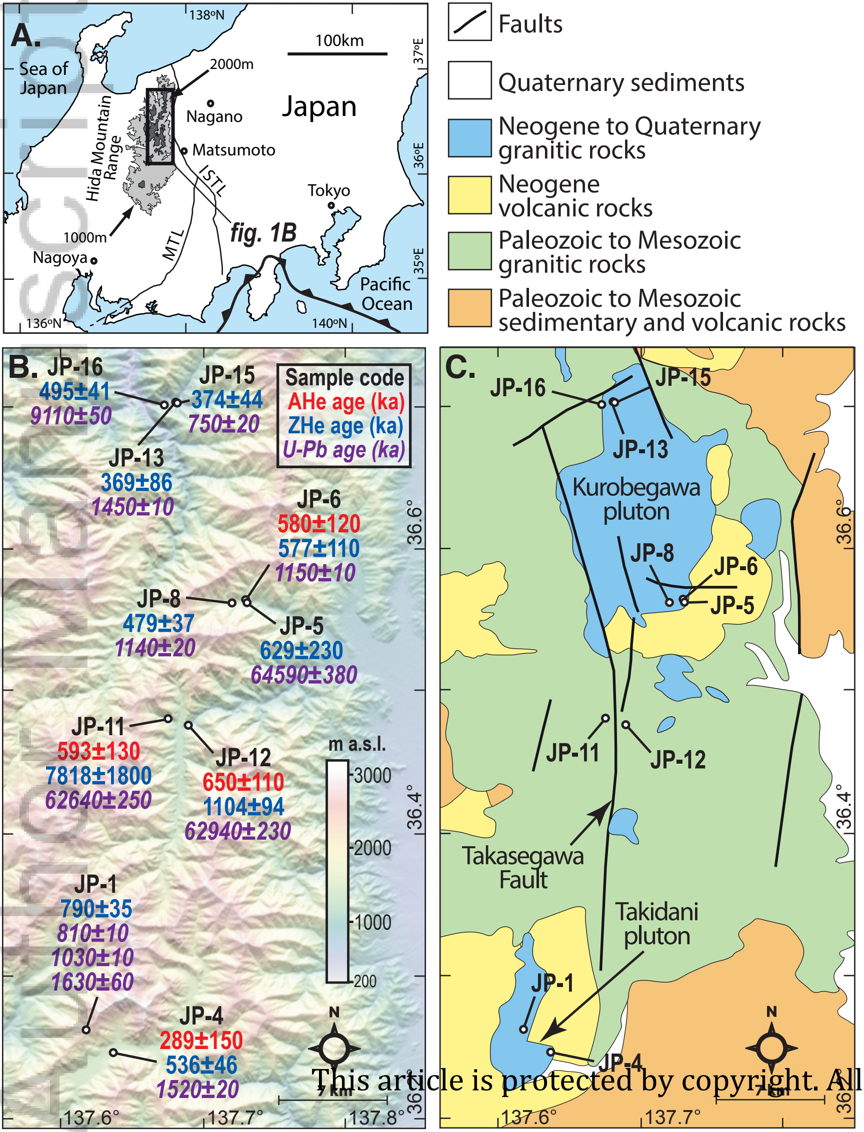
A.
Sea of Japan
Hida Mountain Range
2000m
1000m
Nagano
Matsumoto
Nagoya
Tokyo
Japan
Pacific Ocean
ISTL
MTL
fig. 1B
100km
138ºN
136ºN
140ºN
37ºE
36ºE
35ºE
Faults
Quaternary sediments
Neogene to Quaternary granitic rocks
Neogene volcanic rocks
Paleozoic to Mesozoic granitic rocks
Paleozoic to Mesozoic sedimentary and volcanic rocks
B.
Sample code
AHe age (ka)
ZHe age (ka)
U-Pb age (ka)
JP-16
495±41
9110±50
JP-15
374±44
750±20
JP-13
369±86
1450±10
JP-6
580±120
577±110
1150±10
JP-8
479±37
1140±20
JP-5
629±230
64590±380
JP-11
593±130
7818±1800
62640±250
JP-12
650±110
1104±94
62940±230
JP-1
790±35
810±10
1030±10
1630±60
JP-4
289±150
536±46
1520±20
m a.s.l.
3000
2000
1000
200
N
7 km
137.6°
137.7°
137.8°
36.6°
36.4°
36.2°
C.
JP-16
JP-15
JP-13
Kurobegawa pluton
JP-8
JP-6
JP-5
JP-11
JP-12
Takasegawa Fault
Takidani pluton
JP-1
JP-4
N
7 km
137.6°
137.7°
36.6°
36.4°
36.2°

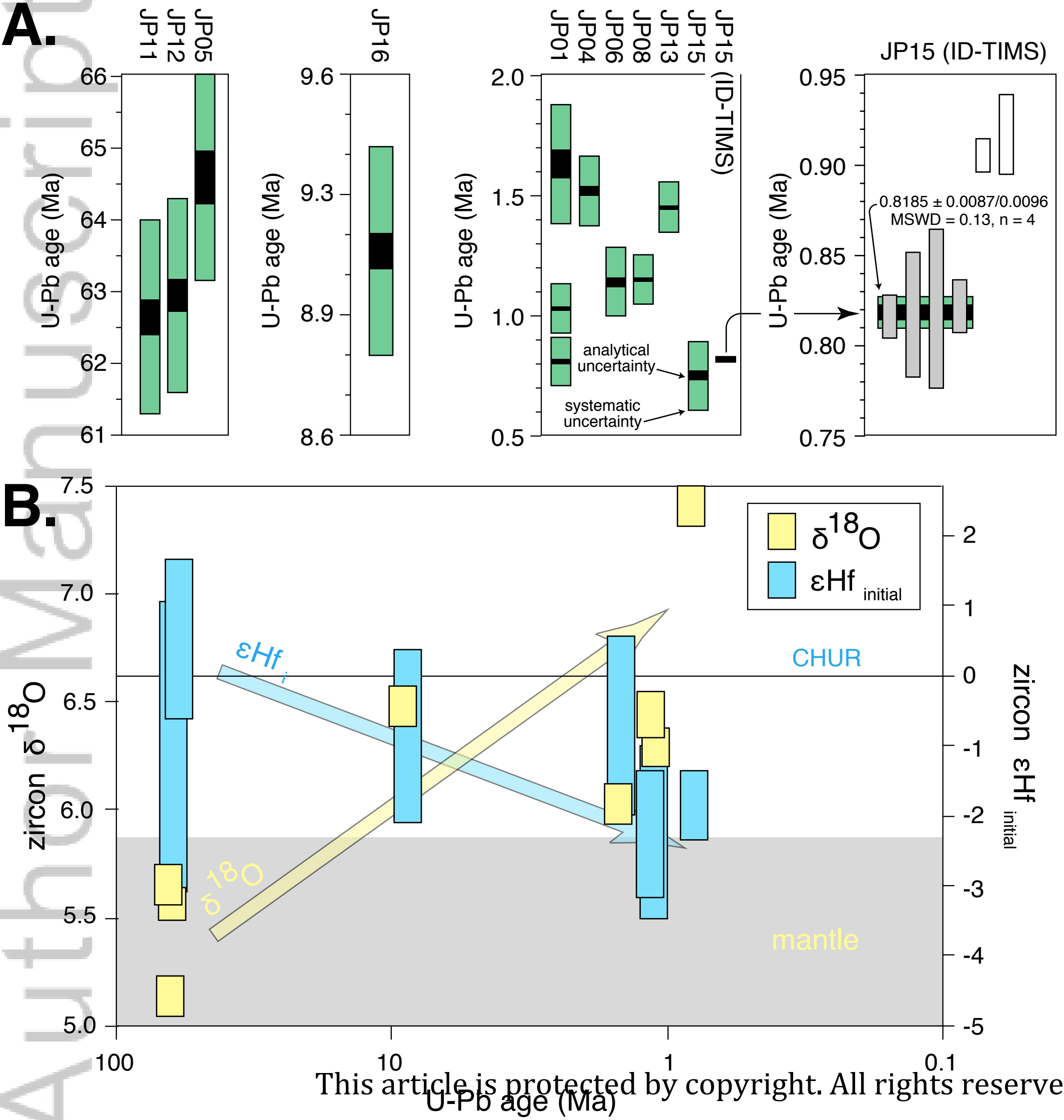
A.
JP11
JP12
JP05
JP16
JP01
JP04
JP06
JP08
JP13
JP15
JP15 (ID-TIMS)
JP15 (ID-TIMS)
U-Pb age (Ma)
66
65
64
63
62
61
9.6
9.3
8.9
8.6
2.0
1.5
1.0
0.5
0.95
0.90
0.85
0.80
0.75
analytical uncertainty
systematic uncertainty
0.8185 ± 0.0087/0.0096
MSWD = 0.13, n = 4
B.
zircon δ18O
7.5
7.0
6.5
6.0
5.5
5.0
δ18O
εHf initial
εHfi
CHUR
mantle
zircon εHf initial
2
1
0
-1
-2
-3
-4
-5
100
10
1
0.1
U-Pb age (Ma)

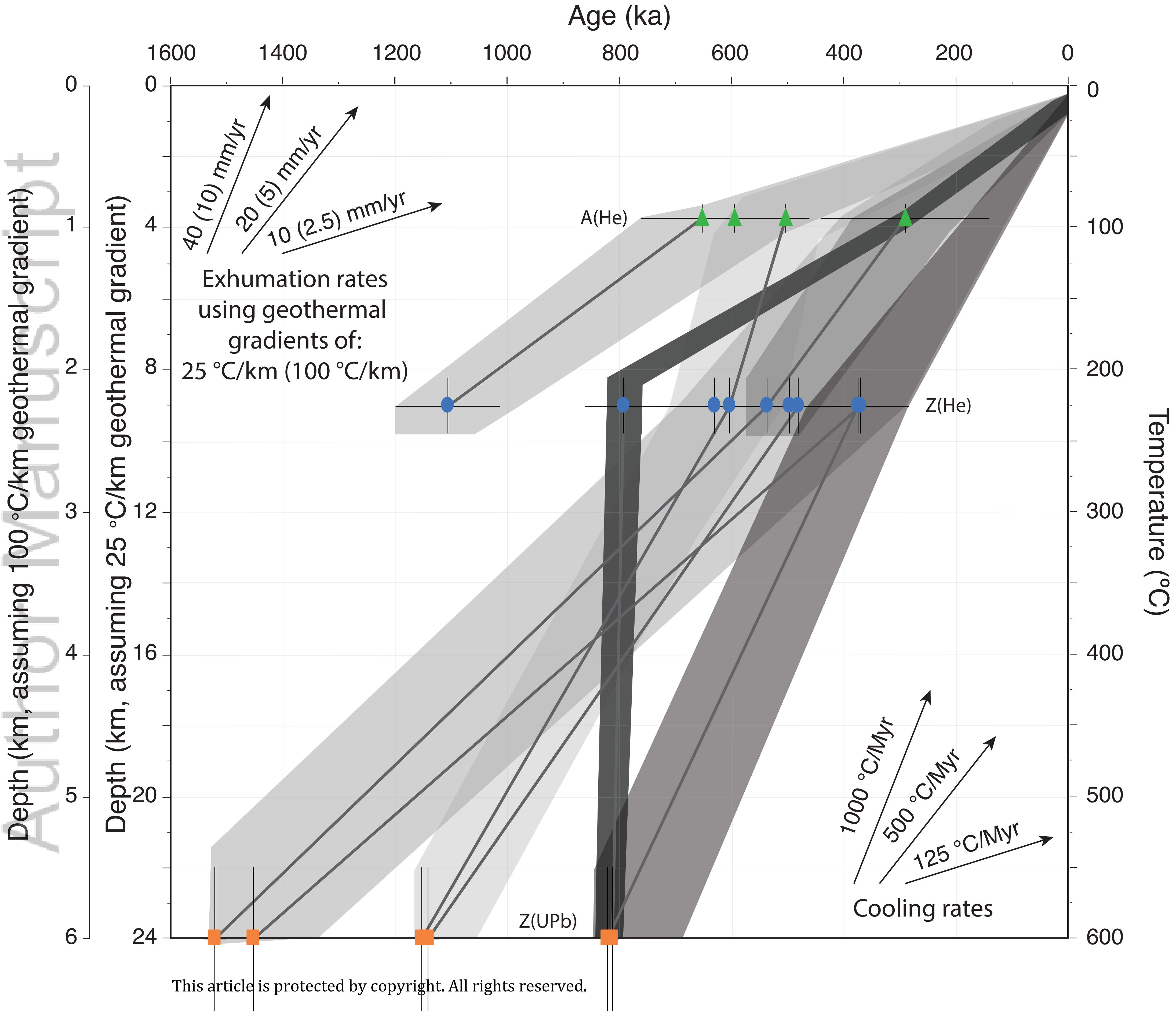
Age (ka)
1600
1400
1200
1000
800
600
400
200
0
Depth (km, assuming 100 °C/km geothermal gradient)
Depth (km, assuming 25 °C/km geothermal gradient)
0
1
2
3
4
5
6
0
4
8
12
16
20
24
Temperature (°C)
0
100
200
300
400
500
600
40 (10) mm/yr
20 (5) mm/yr
10 (2.5) mm/yr
Exhumation rates using geothermal gradients of: 25 °C/km (100 °C/km)
A(He)
Z(He)
Z(UPb)
1000 °C/Myr
500 °C/Myr
125 °C/Myr
Cooling rates

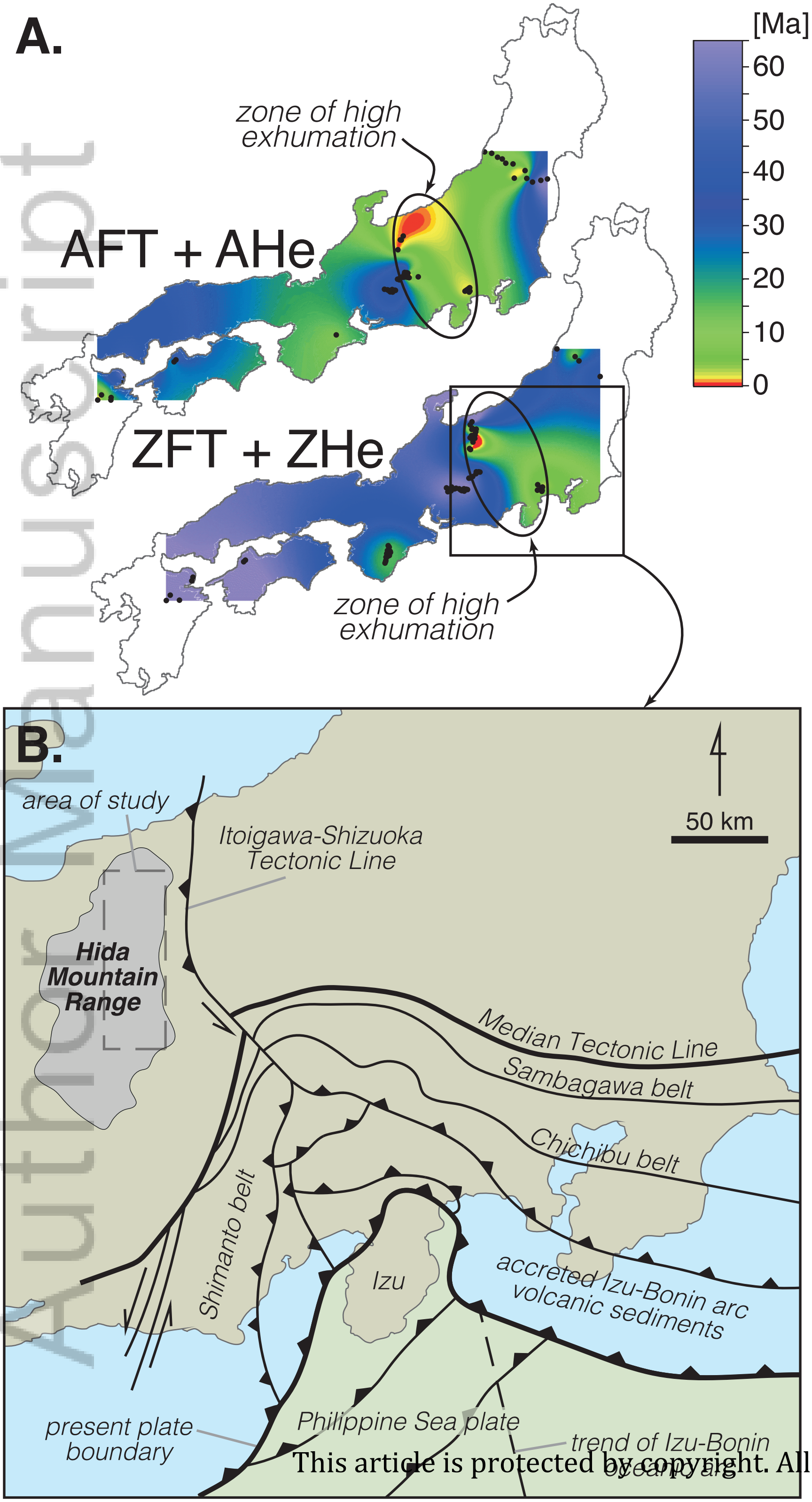
A.
zone of high exhumation
AFT + AHe
ZFT + ZHe
zone of high exhumation
[Ma]
60
50
40
30
20
10
0
B.
area of study
Hida Mountain Range
Itoigawa-Shizuoka Tectonic Line
50 km
Median Tectonic Line
Sambagawa belt
Chichibu belt
Shimanto belt
Izu
accreted Izu-Bonin arc volcanic sediments
present plate boundary
Philippine Sea plate
trend of Izu-Bonin oceanic arc